Temperature driven changes of the graphene edge structure on Ni(111): substrate vs. hydrogen passivation

Laerte L. Patera,[1,2] Federico Bianchini,[1,†] Giulia Troiano,[3] Carlo Dri,[1,2] Cinzia Cepek,[2] Maria Peressi,[1,4,5,] Cristina Africh,[2,*] Giovanni Comelli[1,2,3,6]*

[1] Department of Physics, Università degli Studi di Trieste, via Alfonso Valerio 2, 34127 Trieste, Italy

[2] IOM-CNR Laboratorio TASC, Area Science Park, s.s. 14 km 163.5, Basovizza, 34149 Trieste, Italy

[3] Elettra – Sincrotrone Trieste S.C.p.A. , s.s. 14 km 163.5, Basovizza, 34149 Trieste, Italy

[4] IOM-CNR DEMOCRITOS National Simulation Center Trieste, Italy

[5] Consorzio Interuniversitario Nazionale per la Scienza e la Tecnologia dei Materiali (INSTM), Unità di ricerca di Trieste, piazzale Europa 1, 34128 Trieste, Italy

[6] Center of Excellence for Nanostructured Materials (CENMAT), Università degli Studi di Trieste, via Alfonso Valerio 2, 34127 Trieste, Italy

ABSTRACT

Atomic-scale description of the structure of graphene edges on Ni(111), both *during* and *post* growth, is obtained by scanning tunneling microscopy (STM) in combination with density functional theory (DFT). During growth, at 470°C, fast STM (250 ms/image) evidences graphene flakes anchored to the substrate, with the edges exhibiting *zigzag* or Klein structure depending on the orientation. If growth is frozen, the flake edges hydrogenate and detach from the substrate, with hydrogen reconstructing the Klein edges.

KEYWORDS: graphene, edge, hydrogen, nickel, STM, DFT

TOC Graphics:

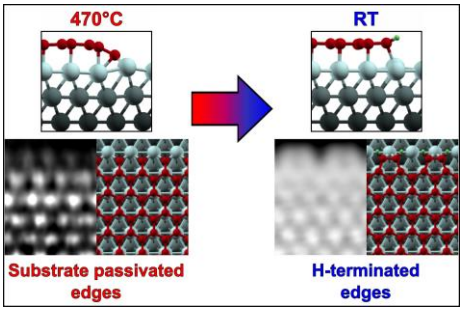

The electronic, magnetic, and chemical properties of graphene and graphitic nanostructures are strongly influenced by the presence and the structure of their edges[1–8]. In free-standing graphene, two main types of edge structures are possible, oriented at 90° from each other: zigzag and armchair[9–13]. Along the zigzag direction, a subset of further reconstructions has been evidenced, both theoretically and experimentally, including: (i) the so-called "5-7" reconstruction, with pentagons/heptagons arranged in a double periodicity[11–15]; (ii) the Klein edge (k), a zigzag edge with an additional carbon bonded to each terminating zigzag C atom[16,17]; (iii) the reconstructed Klein (rk) edge, where the additional C atoms in the k edge bind in couples forming ending pentagons[18,19].

When growing graphene by chemical vapour deposition (CVD), as usually done for large-scale production, the edge morphology, as well as its properties, are strongly influenced by the interaction with the substrate[20–26]. Furthermore, the edge-substrate interaction also plays a major role in the dynamics of graphene formation, steering the growth process[27–30] and the flake orientation[31]. These effects are particularly relevant in case of graphene epitaxial growth on substrates with a small lattice mismatch, as Ni(111) and Co(0001), where the metal surface breaks the symmetry of the hexagonal lattice, thus necessarily yielding two inequivalent structures on adjacent edges of hexagonal islands[32,33]. Recently, Prezzi et al.[33] in a joint theoretical and experimental work nicely demonstrated the presence of zigzag and Klein structures on inequivalent edges on graphene islands on Co(0001). The final C atoms are always placed over surface hollow sites and passivated by the substrate. Inequivalent edges were also experimentally imaged on Ni(111) by Garcia-Lekue et al., and tentatively assigned to zigzag and 5-7 structures[24], although this suggestion was confuted by a more recent theoretical work[32], identifying zigzag and Klein as the most stable structures also on this surface. It has to be noted,

though, that experimental investigations, as well as theoretical calculations, were performed at cryogenic temperatures, i.e. far away both from the conditions relevant for growth and from those relevant for the operation of graphene-based devices.

In this paper, we investigate the atomic structure of graphene edges on Ni(111) both during growth at 470°C and after cooling down to room temperature (RT), by Scanning Tunneling Microscopy (STM) in combination with Density Functional Theory (DFT). For the first time, we unambiguously reveal the effect of residual hydrogen, which is always present in growth processes, on the atomic structure of graphene islands. At 470°C, zigzag (z) and Klein (k) structures form adjacent edges in hexagonal and irregularly shaped islands. We demonstrate that at growth temperatures the edge is passivated by binding to the metal substrate, while upon cooling the flake edges detach from the substrate, most likely due to hydrogenation of the terminal edge C atoms. Furthermore, the binding of H atoms converts the Klein into reconstructed Klein (rk) terminations.

The high-resolution STM image in Figure 1(a) reveals the structure of the two inequivalent adjacent edges of graphene islands over Ni(111) at RT, i.e. in post-growth conditions. Since atomic resolution is achieved here on both the graphene island and the surrounding clean Ni(111), we can place a grid intersecting on top of the metal substrate atoms, as shown in the inset. Extending the grid on the graphene region, we can safely identify the structure of the island as top-fcc, where the bright features in the lower part of the rhombic cells of the grid correspond to C atoms in hollow fcc sites. This is statistically the most abundant configuration on this surface[34]. Looking at the grid, it is also clear that all edges are aligned along the substrate lattice <0-11> and <-101> directions, and terminate with C atoms in hollow (or near-hollow) sites, as for graphene/Co(0001)[33]. Such preference, along with the threefold symmetry of the substrate,

impedes the formation of only zigzag edges, as explained also in ref 32. This is visualized in the schematic model in Figure 1(b): only along three of the six high-symmetry directions of the substrate, a graphene flake can be cut in such a way that its edge is made of terminal C atoms sitting in hollow sites and forming a zigzag with the second line C atoms. In the other three directions, i.e. at the adjacent or opposite sides, the edge with C in hollow results in a Klein geometry. In addition, in the experimental images the Klein geometry seems further reconstructed into a double periodicity configuration, which in principle can be related to both rk and 5-7 edges.

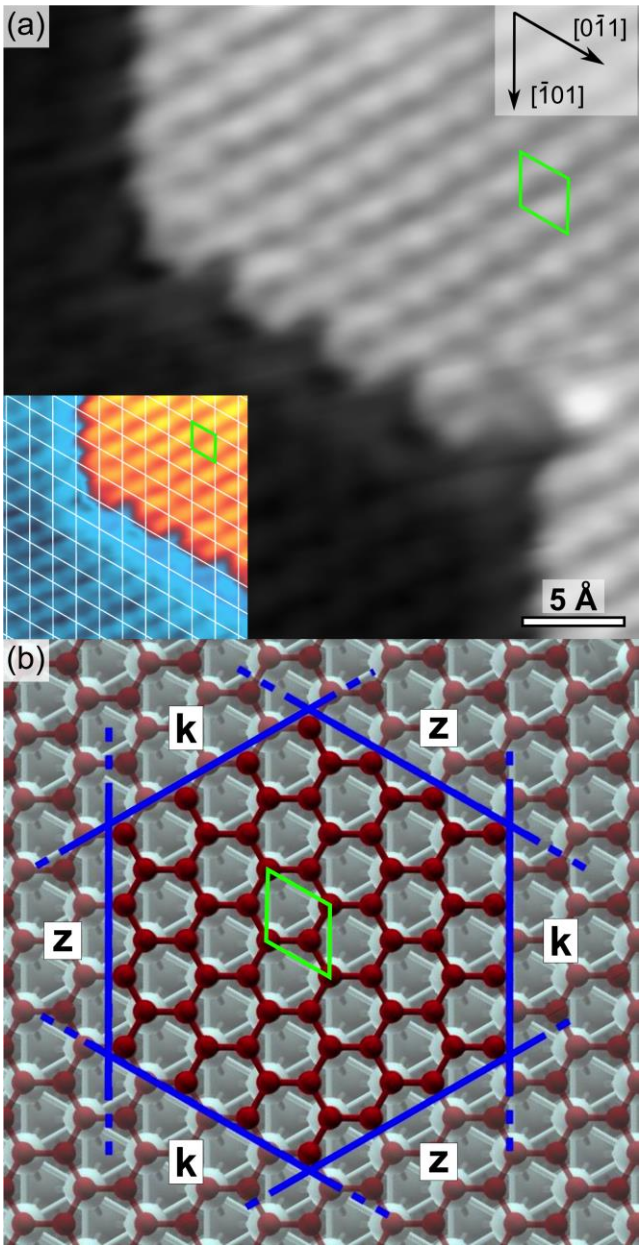

Figure 1. Graphene edges on Ni(111). (a) STM image acquired at RT and showing a graphene island (right) grown on top of a Ni terrace (left) [V=-10mV, I=20nA]. Inset: a grid intersecting on top of the Ni atoms is drawn on a zoom in (a). A two-color scale is used to better highlight the Ni atoms. (b) Stick-and-ball model of a graphene layer on Ni(111). Blue lines indicate cuts passing at hollow C atoms and oriented along the six high-symmetry directions. The expected

inequivalent edges of the resulting graphene island are marked as z (zigzag) and k (Klein). A unit cell is highlighted.

Once clarified the effect of the substrate symmetry on the edge structure, we focus on the detailed analysis of the edge morphology at the atomic level. We first investigate a graphene flake during growth. As we discussed in a previous paper[35], different routes are possible for CVD graphene formation on Ni(111): carbide conversion, embedded growth on clean Ni, seeded growth on top of C-contaminated Ni. It is possible to selectively discriminate between the three routes by a careful control on the CVD parameters (in particular growth temperature and initial substrate contamination). We choose here to follow a seeded growth at 470°C without hydrocarbon exposure, which gives graphene flakes directly growing above the clean Ni substrate, without any intermediate carbide phase, with an average front velocity estimated to be higher than 0.2 nm/s. Due to this high growth speed, a direct imaging of the growing edges with conventional STM scan rates typically achievable by commercial microscopes is impossible. Conversely, our innovative FAST scan system (see Methods) allows us to observe rapidly evolving structures with atomic resolution. In the left column of Figure 2(a) and (c) a frame acquired in 250 ms in quasi-constant height mode (see Methods) on two inequivalent edges is shown. The appearance of the images already suggests that they correspond to z and k edges, respectively. Notably, at variance with the edges imaged at RT (see Figure 1), at 470°C we never see a double periodicity in any edge orientation, which rules out "5-7" and rk reconstructions. The identification of the edge structures as z and k is confirmed by our DFT calculations, which give simulated images in excellent agreement with the experimental ones (central column in Figure 2(a) and (c)). The exclusion of different configurations is further corroborated by the

comparison between experimental and simulated STM images, and by energetics (see Supporting Information). DFT predicts that z and k edges are well stabilized by a strong binding with the substrate of the terminal C atoms in hollow-fcc sites, that bend towards the metal, as clearly visible in the optimized structure of the corresponding stick-and-ball models in Figure 2(a) and (c). The edge–metal bond has a covalent nature, as confirmed not only by the optimized DFT structure, but also by the plot of the calculated electronic charge density shown in Figure 3. A similar effect (i.e. bending induced by the covalent graphene-edge/substrate binding) was observed also on Ir(111)[27], to our knowledge the only previous experimental work probing the edge–metal interaction during growth. The bending at the edges results in a reduced brightness of the last row of C atoms in both simulated and experimental STM images of the edges, regardless of their z or k structure, as for graphene edges on Co(0001) imaged at 4.9 K[33].

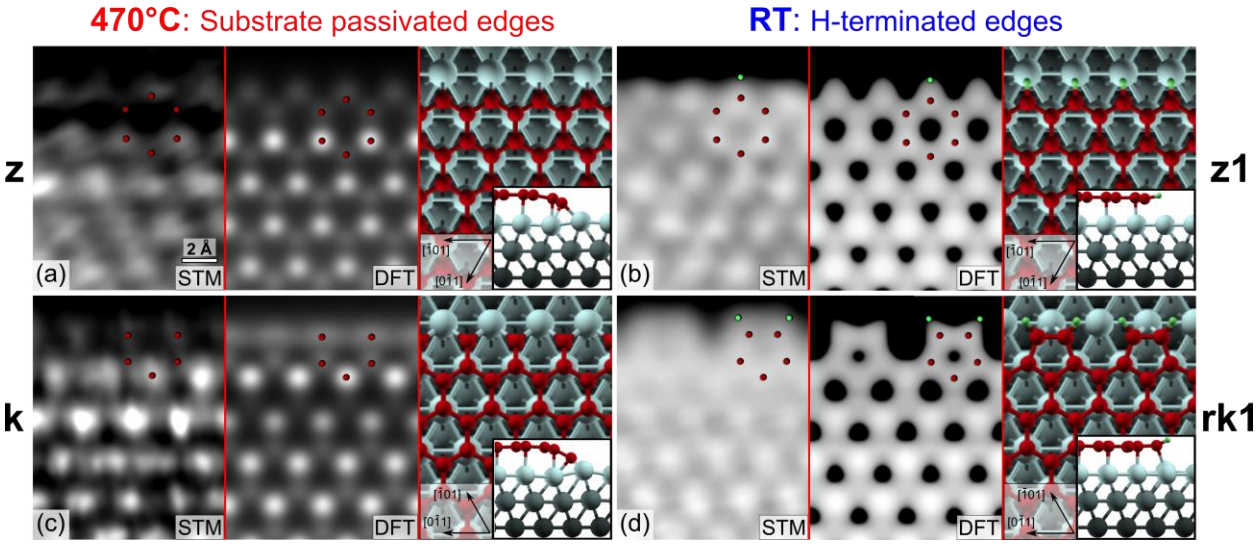

Figure 2. Atomic structure of graphene edges on Ni(111) along the 2 inequivalent directions, imaged at different temperatures. Notice that images and models in (c) and (d) are rotated with respect to images and models in (a) and (b). (a,c) FAST STM images acquired in 250 ms during

growth at 470°C in quasi-constant height mode (left), constant height DFT-simulated images (center) and stick-and-ball models of the calculated geometries (right). (b,d) Post-growth STM images acquired at RT in constant current mode (left), constant current DFT-simulated images (center) and stick-and-ball models of the calculated geometries (right). Scanning parameters: (a,c) experimental parameters: V=+9mV, I=1.3nA; distance of 0.5 Å from graphene for DFT images; (b,d) experimental parameters: V=+200mV, I=20nA; integrated density of states isovalue of 7 10^{-5} $|e|/a^3_0$. for DFT images. In all stick-and-ball models red (grey) balls are C (Ni) atoms, while small green balls are H atoms. On all images red (green) dots are drawn at the position of C (H) atoms.

If the growth is quenched by cooling the sample to RT before completion of the monolayer, supported graphene flakes as that in Figure 1(a) result. Experimental high-resolution STM images acquired in constant current mode at RT (see left column in Figure 2(b) and (d)) reveal the atomic structure of the two inequivalent edges along the directions exhibiting, respectively, z and k geometry at the growth temperature. These images clearly show important differences with respect to the corresponding ones acquired at the growth temperature. Strikingly, this time no reduction of the brightness for the last row of C atoms, but rather a sharp step is observed for both the z and the k edges. Furthermore, along the direction corresponding to k geometry (Figure 2(d)), the protruding hollow C atoms are apparently joined into couples, giving rise to pentagons, suggesting a "5-7" or a rk reconstruction. A closer look at the STM image in comparison with a superimposed stick-and-ball model of the "5-7" geometry allows us to exclude this reconstruction, while the position of the brightest spots is compatible with the rk structure, as evidenced in the figure by the superimposed red dots.

Still, the observed experimental images are not compatible with our simulated images of any kind of "clean" graphene edges passivated by the Ni(111) substrate (for rk imaging see Supporting Information). Thus, in order to retrieve the experimental brightness we have to passivate the edges in a different way. Considering that H_2 is the most abundant contaminant in any UHV system and that graphene edges can be hydrogenated, certainly in free-standing flakes[12,13] but even on metal substrates if exposed to atomic H[36], we examine in details the interaction of the graphene edges with an H_2 molecule. Firstly we consider the possibility that the H_2 molecule is directly trapped and dissociated by the ending C atoms. Our simulations show that indeed dissociation would take readily place if the impinging molecule gets close enough to the edge, but indicate also that the molecule can experience a significant barrier when approaching from the gas phase. A thorough search for a specific low-barrier approaching channel would require extensive calculations that are out of the scope of this work. On the other side, it is well known that the H_2 molecule easily dissociates on the Ni(111) surface[37], with a DFT estimated activation barrier ranging from few meV[38,39] to a maximum of 0.10 eV[40]. Our DFT calculations show that atomic hydrogen can indeed easily access and hydrogenate the graphene edges (see Supporting Information), thus yielding a stable structure with one H atom bound to each terminal C atom. Once hydrogenated, the edge is no longer bent towards the substrate, due to the breaking of the covalent bonds with the metal. This is clearly visible in the optimized structures shown by the stick-and-ball models in Figure 2(b) and (d), in the corresponding calculated charge density plots and atomic projected density of states in Figure 3. The central column in Figure 2(b) shows a simulated image of a hydrogenated z edge (hereafter named z1, with reference to the number of H atoms bound to each terminal C atom). The resemblance with the experimental image is now evident. Even more striking is the effect of the

hydrogenation on the k edge. Here the presence of the H atoms not only breaks the bonds with the metal, but also forces the protruding C atoms to bend towards each other into couples forming closed pentagons, thus turning the "clean" k into a hydrogenated rk (hereafter rk1) edge. Again, the simulated STM image of such structure is in remarkable agreement with the experimental one (compare central and left column in Figure 2(d)). To further support our identification of hydrogenated edges at RT, we want to highlight that combining the available information about H_2 dissociative adsorption on Ni(111) with the results of our simulations for the edge hydrogenation by means of the resulting adsorbed H atoms, we deduce that the overall hydrogenation process of the graphene/Ni(111) edge is exothermic and practically barrierless: an energy gain of more than 1 eV/terminal C atom with respect to the molecule impinging from the gas phase is found, more precisely 1.17 (1.09) eV/terminal C atom for z (k) edges respectively (see Figure 4). It is worth to point out that the hydrogenation process of the edges is favored despite the breaking of the covalent bonds with the substrate acts in the opposite direction, requiring an energy cost. For comparison, the hydrogenation of the z and rk edges in free-standing graphene (where k is not stable) would give a DFT energy gain more than twice as large as in case of adsorption on Ni(111): precisely, 2.65 (2.67) eV/terminal C atom for z (rk) edges, respectively.

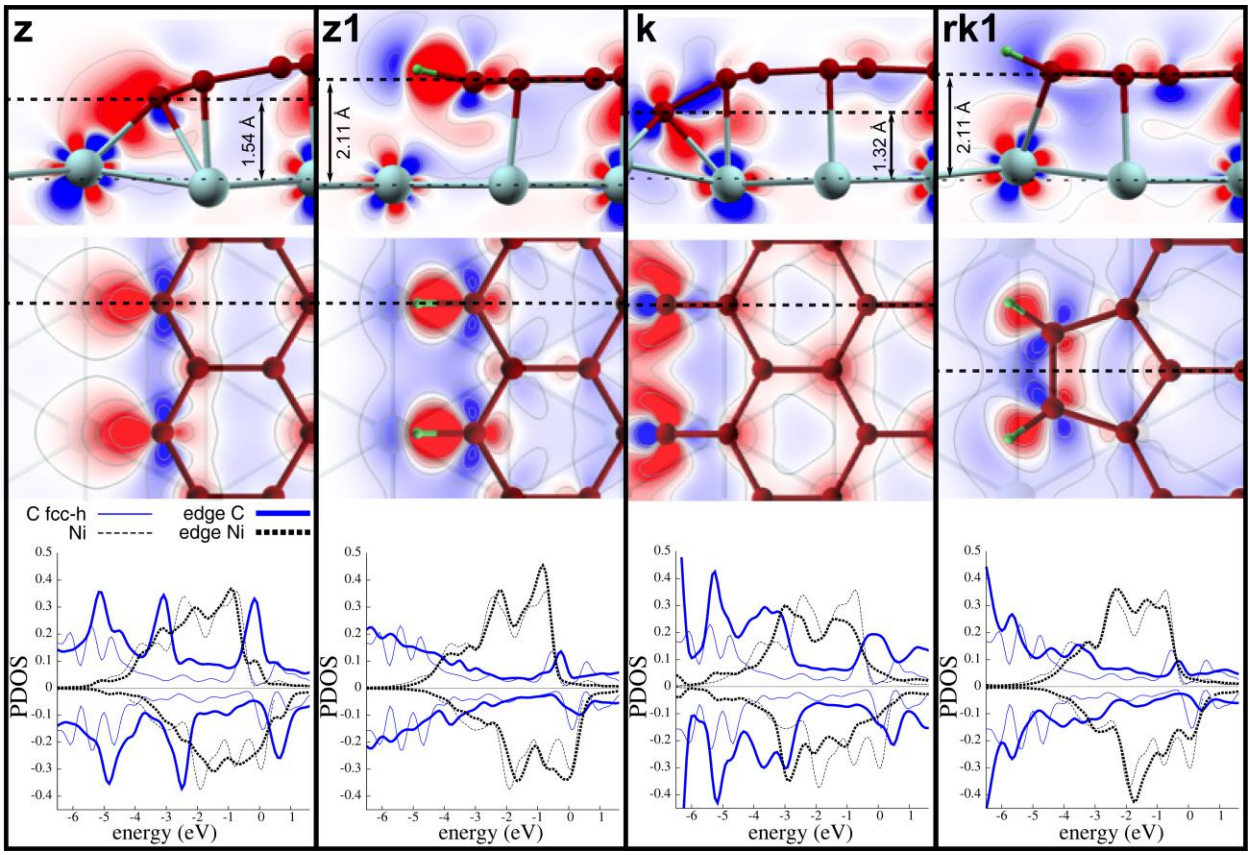

Figure 3. DFT calculated electronic properties of z, z1, k and rk1 graphene edges on Ni(111). Upper and middle panels: electron density difference plots, obtained subtracting the electron density distribution of the graphene and of the substrate calculated separately from that of the total system. For each configuration, side (upper panels) and top (middle panels) views are shown, with the essential parts of the corresponding stick-and-ball models superimposed for reference; dashed lines indicate the planes chosen for the electron density plots; blue/red colors correspond to electron depletion/accumulation ranging from -15 to +15 $\times 10^{-3}|e|/a^3_0$. In the upper panels, the height of the terminal C atoms with respect to the Ni substrate is also indicated. Lower panels: DFT spin-resolved atomic projected density of states (PDOS) of the atoms relevant to the edge. Positive/negative values are for spin up/down.

In Figure 3 we also show the density of states projected onto the atoms relevant to the edge, i.e., onto the terminal edge C atoms (named edge C in figure) and the closest surface Ni atoms (edge Ni). For comparison, the projections onto the C atoms in fcc-hollow site (C fcc-h) and the surface Ni atoms far from the edge (Ni) are also shown, corresponding to those reported in the bottom panel of Figure SI1 of ref 34 for an infinite graphene layer. While in the hydrogen passivated edge (z1 and rk1) only small differences are visible for the terminal C atoms with respect to the infinite layer case, a large variation can be observed in the z and k edges, due to the substrate passivation and in particular to the stronger hybridization with the Ni electronic d-states.

DFT predicts also other stable hydrogenated configurations with a different number of H atoms, whose presence is however excluded when comparing their simulated STM images with experimental ones.

Since H_2 is always present, typically as the most abundant component of the residual atmosphere in all growth chambers, this hydrogenation process is highly probable. Furthermore, the possible existence of hydrogenated graphene edges for CVD graphene in UHV conditions was previously suggested also on the Ir(111) surface[20]. H is strongly bound to the edge C atoms: we imaged the islands at different temperatures in the 25-300°C range after hydrogenation, and they never changed their appearance, always exhibiting a sharp profile and a clear z1 and rk1 geometry. This is in good agreement with the stability of the CH groups at the edges of graphene islands on metal substrates[36] and with the barrier of at least 1 eV predicted by DFT for the dehydrogenation process (right to left in Figure 4 – see also Supporting Information).

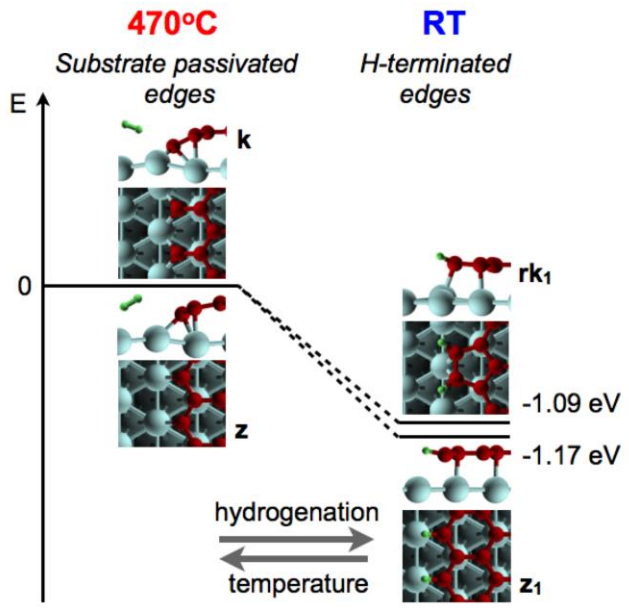

Figure 4. DFT energy diagram of the most favored configurations of graphene edges on Ni(111) upon hydrogenation and dehydrogenation. The dashed lines do not indicate the details of possible hydrogenation/dehydrogenation paths but are just a guide to join z with z1 and k with rk1. Zero energy corresponds to the substrate passivated configurations and H_2 molecules in gas phase; precisely, one molecule for each pair of terminal C atoms of the edge is considered in order to keep the same stoichiometry of the corresponding single-hydrogen passivated configuration; the energy values are reported here per terminal C atom. The DFT calculations are performed at 0K, and the temperature labels refer therefore to the conditions of experimental observations. Zero point energies are not included, since, from the values reported in literature for the H_2 molecule and the H-C bond at the z1 edge[33]), their contribution to the energy differences is not significant.

Upon heating to T>300°C, experiments indicate that the growth process is restored and a complete graphene layer forms. At such temperature, the dehydrogenation barriers predicted by

DFT can be overcome: the C-H bonds break and H_2 molecules form and desorb. Therefore, although the energetics would be unfavorable in presence of hydrogen, upon heating hydrogen is removed and the edge passivation occurs again through the substrate.

Finally, we underline that we investigated the edge structure also during and after growth under hydrocarbon exposure, finding results similar to those presented above, as expected on the basis of our calculations of the ground-state structures with and without hydrogen at the edges.

In conclusion, we demonstrated that temperature acts as a control parameter driving the structure of graphene/Ni(111) edges by changing their passivation. When graphene forms above a Ni(111) substrate (i.e. at T>300°C), during the growth process its edges are clean and anchored to the metal substrate, as predicted by Zhang et al.[30] Growing graphene flakes are thus sealed, most probably thereby hindering the penetration of ad-species below the flake. Upon cooling to RT, the growth is stopped and supported graphene flakes result. The edges of the flakes are now hydrogenated via dissociation of H_2 molecules from the residual background gas pressure. If the growth is carried out under C_2H_4 exposure, residual hydrogen or radicals from hydrocarbon dissociation could also contribute to this process. At RT the flake edges are detached from the substrate, thus potentially favoring the intercalation of other species below graphene. The hydrogenated structure is highly stable upon heating, until the growth process is restored at T>300°C; hydrogen effects have therefore to be taken into account when considering possible applications of graphene flakes on Ni substrates. This mechanism to trap and release hydrogen can in part be responsible for the enhanced hydrogen storage capability in carbon-based nanocomposites[41,42], making sp^2-type edges in direct contact with metals an active site for hydrogen storage at low pressure.

We believe that the comprehension of the edge structures during growth provided here is fundamental to devise better ways to control the growth of regular, defect-free graphene layers on Ni substrates, as well as the formation of hybrid structures. The understanding of the different passivation when changing the temperature can turn into a valuable mean to functionalize graphene flakes as well as to facilitate intercalation.

METHODS. The experiments were performed in a UHV system (base pressure 1×10^{-10} mbar) equipped with standard sample preparation facilities and with an Omicron VT-STM. Epitaxial graphene was prepared on a Ni(111) single crystal by annealing at 400-500°C with or without exposure to ethylene (p =2×10^{-7} mbar). Room temperature STM images were acquired in constant current mode with typical scanning parameters I = 1-30 nA and Vb = ±200 mV. High temperature STM measurements were performed using FAST[43], an innovative add-on module for increasing the imaging frequency of commercial scanning probe microscopes up to video-rate and beyond. In the experiments here discussed, image time-series were acquired in quasi-constant height mode with a frame rate of 4Hz (fast scanning frequency of 800 Hz). This rate allowed us to acquire static images of the graphene edges at 470°C with atomic resolution (I=1-10 nA, Vb = ±200 mV).

Spin-polarized DFT calculations are performed with the plane-wave-based suite Quantum ESPRESSO[44] employing the Generalized Gradient Approximation for the exchange-correlation functional in the Perdew-Burke-Ernzerhof parametrization (GGA-PBE)[45], using ultrasoft pseudopotentials in the Rappe-Rabe-Kaxiras-Joannopoulos formulation[46]. For Ni, the nonlinear core-correction is included, and d states are considered in valence. Semiempirical corrections accounting for the van der Waals interactions are included with the DFT-D approach[47]. A Γ-centered 7x1x1 k-point mesh is typically used for Brillouin zone integration.[48] Other technical

details, such as the smearing parameter[49] and the kinetic energy cutoff for the plane wave basis set, are the same as in ref 34. We use periodically repeated supercells with a 5-layer Ni slab, with a graphene ribbon on one side of the slab. The Ni lattice parameter is used, and the graphene is slightly stretched (the surface lattice mismatch is about 1%). As explained in ref 33, the ribbon has necessarily one edge of type z and the opposite one of type k or rk if terminal C atoms are on fcc-hollow sites. The in-plane periodicity in the direction [-101] or [0-11] is dictated by the edge structure, and therefore it is simply equal to or at most twice the side of the Ni(111) surface unit cell. In the direction orthogonal to the edge, the period is much longer in order to isolate parallel edges, both those pertaining to the same ribbon and those pertaining to two adjacent ribbons, separated by a region of clean Ni surface. We use ribbons 4.2 nm large, corresponding to 39 rows of C atoms, with periodically repeated images separated by 1.4 nm, to ensure that the central part of the ribbon recovers the features of the infinite graphene layer, and that the central part of the clean Ni region has the same appearance of a clean Ni surface in the simulated STM image. The graphene ribbon and the last three Ni layers are allowed to relax when optimizing the atomic positions.

STM images are simulated within the Tersoff-Hamann approximation[50], according to which the tunneling current is proportional to the energy-Integrated electronic Local Density of States (ILDOS). Specifically, we use the conventional cutting of the ILDOS at a constant height to simulate the quasi-constant height mode of FAST STM scan. Instead, in order to mimic the constant-current experimental STM images acquired post-growth, we map an ILDOS iso-surface lying within a certain height range over the graphene. Ball models are rendered with the XCrySDen software[51].

The energy gain upon hydrogenation is estimated calculating the difference of the total energies of two systems that differ for the configuration of only one of the two edges due to the hydrogen atoms, whereas the other edge is the same: in one case the hydrogen atoms are in gas phase, in the other are adsorbed on the edge. Zero point energies are not included, since they would add only a small correction to the energy gain.

ASSOCIATED CONTENT

Supporting Information. The analysis of additional possible edge structures, as well as more details on the hydrogenation process, the thermodynamics of the different systems, and the convergence of energetics, structural and electronic properties with the ribbons width. This material is available free of charge via the Internet at http://pubs.acs.org.

AUTHOR INFORMATION

Corresponding Authors

*africh@iom.cnr.it (experiments), peressi@ts.infn.it (theory)

Present Addresses

† Physics Department, King's College London, Strand, London, WC2R 2LS, United Kingdom

Author Contributions

L.L.P., C.C. and C.A. conceived and designed the experiments. L.L.P. performed all the experiments. F.B. and M.P. conceived and designed the calculations. F.B. performed the calculations. G.T. and C.D. contributed to the FAST STM measurements. L.L.P., F.B., M.P. and

C.A. analyzed the data and discussed the results. C.A, M.P and G.C. co-wrote the paper. All authors have given approval to the final version of the manuscript.

Notes

The authors declare no competing financial interests.

ACKNOWLEDGMENT

L.L.P. acknowledges funding from MIUR through Progetto Strategico NFFA. C.A. and C.C. acknowledge support from MIUR through the program PRIN 2010-2011 – Project nº 2010N3T9M4 and the program `Progetto Premiale 2012' - Project ABNANOTECH. Computational resources have been partly obtained through Italian SuperComputing Resource Allocation (ISCRA) grants of the Consorzio Interuniversitario CINECA, partly within the agreement between the University of Trieste and CINECA. L.L.P., C.C. and C.A. acknowledge Stephan Hofmann and Robert S. Weatherup for introducing the scientific question and for fruitful discussion.

REFERENCES

(1) Castro Neto, A. H.; Guinea, F.; Peres, N. M. R.; Novoselov, K. S.; Geim, A. K. *Rev. Mod. Phys.* **2009**, *81*, 109–162.

(2) Ritter, K. A.; Lyding, J. W. *Nat. Mater.* **2009**, *8*, 235–242.

(3) Fujii, S.; Enoki, T. *Acc. Chem. Res.* **2012**, *46*, 2202–2210.

(4) Lee, H.; Son, Y.-W.; Park, N.; Han, S.; Yu, J. *Phys. Rev. B* **2005**, *72*, 174431.

(5) Yazyev, O.; Katsnelson, M. *Phys. Rev. Lett.* **2008**, *100*, 047209.

(6) Ohtsuka, M.; Fujii, S.; Kiguchi, M.; Enoki, T. *ACS Nano* **2013**, *8*, 6868–6874.

(7) Hod, O.; Barone, V.; Peralta, J. E.; Scuseria, G. E. *Nano Lett.* **2007**, *7*, 2295–2299.

(8) Jiang, D.; Sumpter, B. G.; Dai, S. *J. Chem. Phys.* **2007**, *126*, 134701.

(9) Rozhkov, A. V.; Giavaras, G.; Bliokh, Y. P.; Freilikher, V.; Nori, F. *Phys. Rep.* **2011**, *503*, 77–114.

(10) Kawai, T.; Miyamoto, Y.; Sugino, O.; Koga, Y. *Phys. Rev. B* **2000**, *62*, R16349–R16352.

(11) Girit, Ç. Ö.; Meyer, J. C.; Erni, R.; Rossell, M. D.; Kisielowski, C.; Yang, L.; Park, C.-H.; Crommie, M. F.; Cohen, M. L.; Louie, S. G.; Zettl, A. *Science* **2009**, *666*, 1705–1708.

(12) Wassmann, T.; Seitsonen, A. P.; Saitta, A. M.; Lazzeri, M.; Mauri, F. *Phys. Rev. Lett.* **2008**, *101*, 096402.

(13) Wassmann, T.; Seitsonen, A. P.; Saitta, A. M.; Lazzeri, M.; Mauri, F. *Phys. Status Solidi* **2009**, *246*, 2586–2591.

(14) Koskinen, P.; Malola, S.; Häkkinen, H. *Phys. Rev. Lett.* **2008**, *101*, 115502.

(15) Koskinen, P.; Malola, S.; Häkkinen, H. *Phys. Rev. B* **2009**, *80*, 073401.

(16) Klein, D. J. *Chem. Phys. Lett.* **1994**, *217*, 261–265.

(17) Kobayashi, Y.; Fukui, K.; Enoki, T.; Kusakabe, K. *Phys. Rev. B* **2006**, *73*, 125415.

(18) Ivanovskaya, V. V.; Zobelli, A.; Wagner, P.; Heggie, M. I.; Briddon, P. R.; Rayson, M. J.; Ewels, C. P. *Phys. Rev. Lett.* **2011**, *107*, 065502.

(19) Ivanovskaya, V. V; Wagner, P.; Zobelli, A.; Suarez-Martinez, I.; Yaya, A.; Ewels, C. P. *Graph. 2011* **2012**, 75–85.

(20) Li, Y.; Subramaniam, D.; Atodiresei, N.; Lazic, P.; Caciuc, V.; Pauly, C.; Georgi, A.; Busse, C.; Liebmann, M.; Blügel, S.; Pratzer, M.; Morgenstern, M.; Mazzarello, R. *Adv. Mater.* **2013**, *25*, 1967–1972.

(21) Subramaniam, D.; Libisch, F.; Li, Y.; Pauly, C.; Geringer, V.; Reiter, R.; Mashoff, T.; Liebmann, M.; Burgdörfer, J.; Busse, C.; Michely, T.; Mazzarello, R.; Pratzer, M.; Morgenstern, M. *Phys. Rev. Lett.* **2012**, *108*, 046801.

(22) Phark, S.-H.; Borme, J.; Vanegas, A. L.; Corbetta, M.; Sander, D.; Kirschner, J. *ACS Nano* **2011**, *5*, 8162–8166.

(23) Tian, J.; Cao, H.; Wu, W.; Yu, Q.; Chen, Y. P. *Nano Lett.* **2011**, *11*, 3663–3668.

(24) Garcia-Lekue, A.; Balashov, T.; Olle, M.; Ceballos, G.; Arnau, A.; Gambardella, P.; Sanchez-Portal, D.; Mugarza, A. *Phys. Rev. Lett.* **2014**, *112*, 066802.

(25) Gao, J.; Zhao, J.; Ding, F. *J. Am. Chem. Soc.* **2012**, *134*, 6204–6209.

(26) Olle, M.; Ceballos, G.; Serrate, D.; Gambardella, P. *Nano Lett.* **2012**, *12*, 4431–4436.

(27) Lacovig, P.; Pozzo, M.; Alfè, D.; Vilmercati, P.; Baraldi, A.; Lizzit, S. *Phys. Rev. Lett.* **2009**, *103*, 166101.

(28) Artyukhov, V. I.; Liu, Y.; Yakobson, B. I. *Proc. Natl. Acad. Sci. U. S. A.* **2012**, *109*, 15136–15140.

(29) Shu, H.; Chen, X.; Tao, X.; Ding, F. *ACS Nano* **2012**, *6*, 3243–3250.

(30) Zhang, X.; Wang, L.; Xin, J.; Yakobson, B. I.; Ding, F. *J. Am. Chem. Soc.* **2014**, *136*, 3040–3047.

(31) Zhang, X.; Xu, Z.; Hui, L.; Xin, J.; Ding, F. *J. Phys. Chem. Lett.* **2012**, *3*, 2822–2827.

(32) Artyukhov, V.; Hao, Y.; Ruoff, R.; Yakobson, B. *arXiv Prepr. 1405.5799v1* **2014**, 1–14.

(33) Prezzi, D.; Eom, D.; Rim, K. T.; Zhou, H.; Xiao, S.; Nuckolls, C.; Heinz, T. F.; Flynn, G. W.; Hybertsen, M. S. *ACS Nano* **2014**, *6*, 5765–5773.

(34) Bianchini, F.; Patera, L. L.; Peressi, M.; Africh, C.; Comelli, G. *J. Phys. Chem. Lett.* **2014**, *5*, 467–473.

(35) Patera, L. L.; Africh, C.; Weatherup, R. S.; Blume, R.; Bhardwaj, S.; Castellarin-Cudia, C.; Knop-Gericke, A.; Schloegl, R.; Comelli, G.; Hofmann, S.; Cepek, C. *ACS Nano* **2013**, *7*, 7901–7912.

(36) Dinger, A.; Lutterloh, C.; Biener, J.; Küppers, J. *Surf. Sci.* **1999**, *421*, 17–26.

(37) Robota, H. J.; Vielhaber, W.; Lin, M. C.; Segner, J.; Ertl, G. *Surf. Sci.* **1985**, *155*, 101–120.

(38) Kresse, G. *Phys. Rev. B* **2000**, *62*, 8295–8305.

(39) Liu, B.; Lusk, M. T.; Ely, J. F. *J. Phys. Chem. C* **2009**, *113*, 13715–13722.

(40) Yang, H.; Whitten, J. L. *J. Chem. Phys.* **1993**, *98*, 5039–5049.

(41) Candelaria, S. L.; Shao, Y.; Zhou, W.; Li, X.; Xiao, J.; Zhang, J.-G.; Wang, Y.; Liu, J.; Li, J.; Cao, G. *Nano Energy* **2012**, *1*, 195–220.

(42) Choi, M. H.; Min, Y.-J.; Gwak, G.-H.; Paek, S.-M.; Oh, J.-M. *J. Alloys Compd.* **2014**, *610*, 231–235.

(43) Esch, F.; Dri, C.; Spessot, A.; Africh, C.; Cautero, G.; Giuressi, D.; Sergo, R.; Tommasini, R.; Comelli, G. *Rev. Sci. Instrum.* **2011**, *82*, 053702.

(44) Giannozzi, P.; Baroni, S.; Bonini, N.; Calandra, M.; Car, R.; Cavazzoni, C.; Ceresoli, D.; Chiarotti, G. L.; Cococcioni, M.; Dabo, I.; Dal Corso, A.; de Gironcoli, S.; Fabris, S.; Fratesi, G.; Gebauer, R.; Gerstmann, U.; Gougoussis, C.; Kokalj, A.; Lazzeri, M.; Martin-Samos, L.; Marzari, N.; Mauri, F.; Mazzarello, R.; Paolini, S.; Pasquarello, A.; Paulatto, L.; Sbraccia, C.; Scandolo, S.; Sclauzero, G.; Seitsonen, A. P.; Smogunov, A.; Umari, P.; Wentzcovitch, R. M. *J. Phys. Condens. Matter* **2009**, *21*, 395502.

(45) Perdew, J.; Burke, K.; Ernzerhof, M. *Phys. Rev. Lett.* **1996**, *77*, 3865–3868.

(46) Rappe, A.; Rabe, K.; Kaxiras, E.; Joannopoulos, J. *Phys. Rev. B* **1990**, *41*, 1227–1230.

(47) Grimme, S. *J. Comput. Chem.* **2006**, *27*, 1787–1799.

(48) Monkhorst, H. J.; Pack, J. D. *Phys. Rev. B* **1976**, *13*, 5188–5192.

(49) Methfessel, M.; Paxton, A. *Phys. Rev. B* **1989**, *40*, 3616–3621.

(50) Tersoff, J.; Hamann, D. *Phys. Rev. B* **1985**, *31*, 805–813.

(51) Kokalj, A. *J. Mol. Graph. Model.* **1999**, *17*, 176–179.